

Structural, Electrical and Dielectric Properties of Hexa-ferrite-Polyaniline Nano-composites

Muhammad Ajmal¹ · M. U. Islam¹ · Absar Ali¹

Received: 26 August 2017 / Accepted: 7 September 2017 / Published online: 12 September 2017
© Springer Science+Business Media, LLC 2017

Abstract Ferrite-polyaniline (PANI) composites were prepared by in situ polymerization of polyaniline with the general formula $(1 - x)$ ferrite + (x) PANI where $x = 0, 0.25, 0.5, 0.75, 1$. The samples were characterized by XRD, SEM, electrical resistivity, and dielectric measurements. X-ray diffraction reveals single phase formation of $\text{CaBaCo}_2\text{Al}_{0.5}\text{Fe}_{11.5}\text{O}_{22}$ Y-type ferrite, whereas polyaniline exhibits an amorphous nature. At room temperature, the resistivity of nano-composites increases with the increase of ferrite filler contents from 3.17×10^4 to $3.19 \times 10^7 \Omega \text{ cm}$. Real and imaginary parts of the complex permittivity of the PANI-ferrite composites follow the Maxwell-Wagner model. Based on the Jonscher Law, the AC conductivity of PANI-ferrite composites experiences an increase with the increase in frequency. The exponent calculated from AC conductivity reveals that the hopping is the likely conduction mechanism. The activation energy obtained from temperature-dependent measurements is consistent with room temperature resistivity. Due to the light weight, low cost and flexibility of design, the ferrite-polymer composites are considered useful for microwave devices.

Keywords Sol–gel · Ferrite-polymer composite · Dielectric constant · Activation energy · AC conductivity

1 Introduction

Today nano-composites are functional materials for modern devices, having versatile physical and chemical properties. Such composites are prepared through the dispersion of magnetic filler particles in the polymer matrix. The filler-polymer properties, filler concentration, and mutual orientation of the filler particles are responsible for the specific properties of composites [1]. Presently, the demand for multifunctional composites is increasing to fulfill the future requirements of electronics components. Owing to their tunable properties, flexibility, and easy fabrication, the ferrite-polymer composites (FPC) have got top importance in electronics [2]. The demand for polyaniline (PANI) as a conducting polymer is increasing because of its easy preparation and reasonable chemical stability. At the protonated state, it shows dramatic changes in physical characteristics and electric structure. It also exhibits high stability in air and is soluble in various solvents [3]. Various high-tech applications, such as satellite TV, sensors, solar cells, electromagnetic shields, energy reservoirs, heating systems, and electro-optical devices, make use of polymer-based composites possessing electro-conductive properties [4]. It is observed that the properties of Y-type hexa-ferrites are close to that of soft ferrites. Hence, the cutoff frequency of Y-type hexa-ferrites is \sim few gigahertz [5]. Moreover, the compact phase shift devices, including electromagnetic interference suspension, chip electronic components (MLCB and MLCI), and the air traffic control systems, also make use of the Y-type hexa-ferrites [5]. In the present study, the Y-type hexagonal ferrite was used with composition $\text{CaBaCo}_2\text{Al}_{0.5}\text{Fe}_{11.5}\text{O}_{22}$ as filler in the PANI matrix. The ferrite-PANI composites with three different combinations

✉ Muhammad Ajmal
m.ajmal507@yahoo.com

¹ Department of Physics, Bahauddin Zakariya University, Multan, 60800, Pakistan

of ferrite, i.e., FP1 (75 wt% of ferrite), FP2 (50 wt% of ferrite), and FP3 (25 wt% of ferrite), were synthesized by in situ polymerization of PANI and thoroughly investigated.

2 Materials and Methods

2.1 Chemicals

Analytical grade reagents $\text{Fe}(\text{NO}_3)_2 \cdot 9\text{H}_2\text{O}$, $\text{Ba}(\text{NO}_3)_2 \cdot 3\text{H}_2\text{O}$, $\text{Co}(\text{NO}_3)_2 \cdot 6\text{H}_2\text{O}$, $\text{Ca}(\text{NO}_3)_2$, $\text{Al}(\text{NO}_3)_3 \cdot 3\text{H}_2\text{O}$, citric acid $\text{C}_3\text{H}_4\text{OH}(\text{COOH})_3$, NH_3 solution and methanol were used as the starting materials. The NH_3 solution and methanol were used as precipitating solution and washing agent respectively. The polyaniline monomer was taken by in situ polymerization.

2.2 Synthesis of $\text{CaBaCo}_2\text{Al}_{0.5}\text{Fe}_{11.5}\text{O}_{22}$ Y-Type Hexa-ferrite

The sol-gel auto combustion method was used to synthesize $\text{CaBaCo}_2\text{Al}_{0.5}\text{Fe}_{11.5}\text{O}_{22}$ hexa-ferrite. The stoichiometric amounts of solutions of iron nitrate $\text{Fe}(\text{NO}_3)_2$ (0.1 M), calcium nitrate $\text{Ca}(\text{NO}_3)_2$ (0.0166 M), cobalt nitrate $\text{Co}(\text{NO}_3)_2$ (0.0166 M), aluminum nitrate $\text{Al}(\text{NO}_3)_3$ (0.0166), barium nitrate $\text{Ba}(\text{NO}_3)_2$ (0.0166 M), and citric acid (0.1998 M) were dissolved in deionized water. The above molar solutions were mixed in a 1000-ml beaker. The ammonia solution (2 M) was added with continuous stirring to maintain $\text{pH} = 7$. The solution was heated at 80°C with continuous stirring to be converted into viscous gel followed by heating at 360°C to convert the gel into ash. In order to obtain homogeneous material, the ash was ground using a pestle and mortar then sintered at 1000°C for 5 h. The powder was pelletized under the force of 30 kN.

2.3 Synthesis of Ferrite-PANI Composites by In Situ Polymerization of PANI

The detailed synthesis of polyaniline (PANI) was reported in our previous study [20]. To synthesize composites, stoichiometric amounts of aniline monomer and ferrite filler were mixed in the required amount of HCl. The APS ammonium peroxydisulfate $[(\text{NH}_4)_2\text{S}_2\text{O}_8]$ solution was slowly added into the aniline solution, and the stirring continued for about an hour. It became thick and greenish in color. A calculated amount of sintered powder (filler) was added into the required amount of aniline with continuous stirring for 1 h. The final greenish solution was kept at room temperature for 24 h. After a repeated filtration process, the filtered sample was dried in an oven at 60°C for 24 h. A mortar and pestle was used to grind the dried powder. Finally,

the force of 30 kN was used to make pellets of composite materials.

3 Results and Discussion

3.1 X-ray Diffraction

The phase purity was checked using X-ray diffraction at room temperature. Figure 1 shows the XRD patterns of the samples. A computer-controlled JDX-3532 JEOL Japan model, operating at 40 KV and 30 mA, was used to record X-ray diffraction patterns. The $\text{CuK}\alpha$ ($\lambda = 1.5406 \text{ \AA}$) radiations were used with a Ni filter, and the scanning of the sample was done in 2θ range 20 to 70° . The comparison of all the peaks of X-ray diffraction patterns of $\text{CaBaCo}_2\text{Al}_{0.5}\text{Fe}_{11.5}\text{O}_{22}$ Y-type ferrite was done with JCPDS card No 00-019-019-0100. It was observed that $\text{CaBaCo}_2\text{Al}_{0.5}\text{Fe}_{11.5}\text{O}_{22}$ reveals a single-phase Y-type structure. The X-ray diffraction patterns also showed that both the phases of $\text{CaBaCo}_2\text{Al}_{0.5}\text{Fe}_{11.5}\text{O}_{22}$ and PANI co-existed in the composite samples. The appearance of peaks of $\text{CaBaCo}_2\text{Al}_{0.5}\text{Fe}_{11.5}\text{O}_{22}$ in all the compositions of PANI confirms the presence of ferrite particles in the polymer matrix. Owing to the amorphous behavior of polyaniline, there is a decrease in the peaks' intensity in the composites [6].

Scherer's formula [7] was used for the calculation of the crystallite size for each sample from the X-ray diffraction pattern as given below

$$D = k\lambda / \beta \cos \theta_B \quad (1)$$

where k is the shape constant with the value 0.89 for the hexagonal system, whereas λ is the wavelength of $\text{CuK}\alpha$ radiation $\lambda = 1.5406 \text{ \AA}$. β is the broadening of the

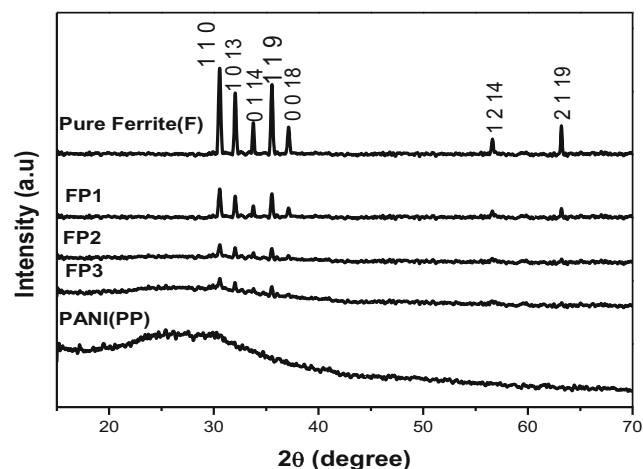


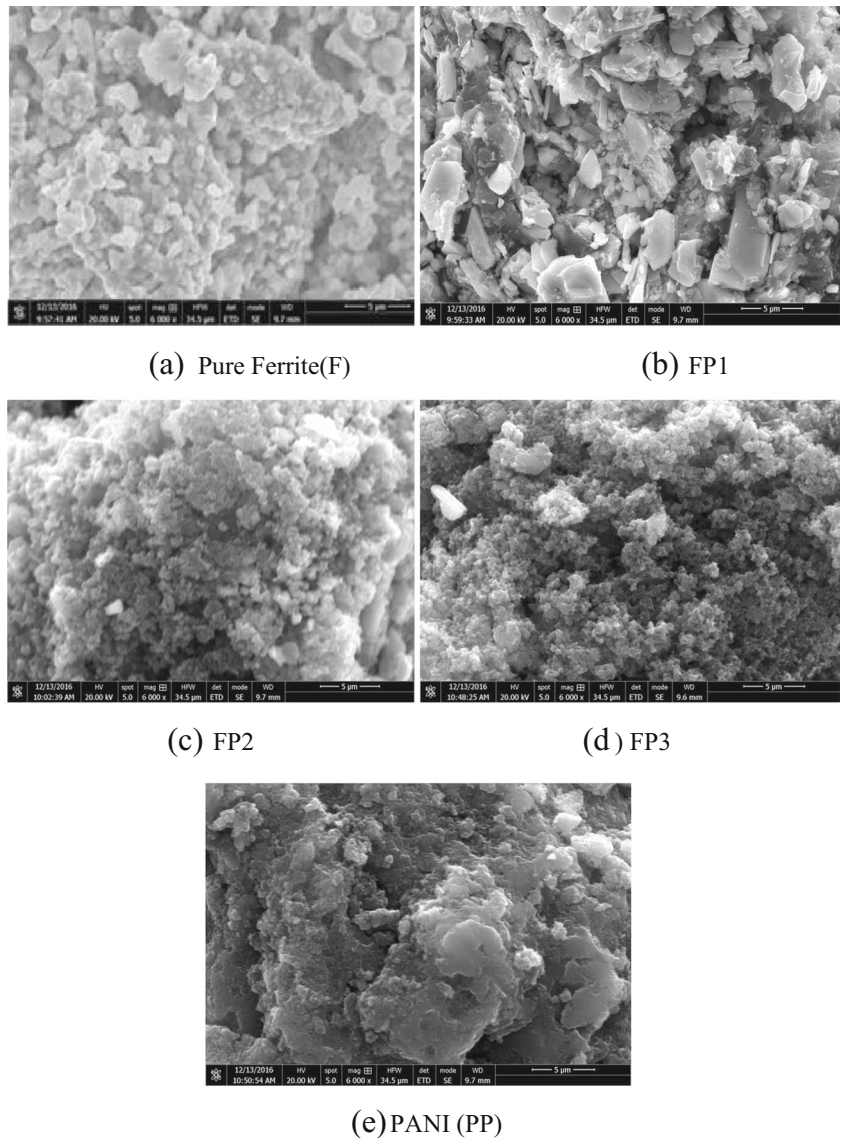
Fig. 1 X-ray diffraction patterns of $\text{CaBaCo}_2\text{Al}_{0.5}\text{Fe}_{11.5}\text{O}_{22}$ (F), FP1, FP2, FP3, and PANI (PP)

Table 1 Lattice constants and cell volume of the unit cell of the synthesized samples

Composition	<i>a</i> (Å)	<i>c</i> (Å)	<i>c/a</i>	<i>V</i> (Å ³)
PF	5.91	43.21	7.311	1307
FP1	5.93	43.42	7.322	1322.26
FP2	5.94	43.53	7.328	1330.08
FP3	5.97	43.32	7.256	1337.07

diffraction line, the measurement of which has been taken at the half width of maximum intensity. θ_B stands for Bragg’s angle of diffraction. The crystallite size of pure ferrite measured was equal to 54.68 nm. It is larger as compared with the size of ferrite-PANI composites. The grain size increases with the decrease in the density of the grain boundary [8].

Fig. 2 SEM profiles of **a** pure ferrite (F), **b** FP1, **c** FP2, **d** FP3, and **e** PANI (PP)



Hence, the grain boundary mobility can be considered as the possible reason for the increase in the grain size.

The volume of the unit cell and Lattice constants *a* and *c* were calculated using (2) and (3) for ferrite and composites [9].

$$\sin^2 \theta = \lambda^2/3a^2(h^2 + thk + k^2) + (\lambda^2/4c^2)l^2 \tag{2}$$

$$V = 0.8666a^2c \tag{3}$$

The volume of the unit cell and calculated values of lattice parameters are tabulated in Table 1. The *c/a* ratio falls into the desired range of the Y-type structure.

3.2 Scanning Electron Microscopy

Figure 2 shows the scanning electron microscopy (SEM) for (a) ferrite CaBaCo₂Al_{0.5}Fe_{11.5}O₂₂(F), (b) FP1, (c) FP2,

(d) FP3, and (e) PANI(PP). It can be observed that the Y-type hexagonal ferrite shows a homogenous structure with hexagonal patterns. With the increase in the ferrite content, the irregular and porous surface morphology of polyaniline changes. The ferrite particles can be seen tucked into the polyaniline matrix. The phase contrast shown by the SEM profile of ferrite-polyaniline composites is conspicuous, whereas the darker phase corresponds to polyaniline and the bright phase to ferrite.

3.3 Dielectric Properties

3.3.1 Dielectric Constant

The following formula was used to calculate the dielectric constant (ϵ') from the measured value of the capacitor [12]:

$$\epsilon' = Cd/A\epsilon_0 \quad (4)$$

The variation of the dielectric constant (ϵ') vs frequency (20 Hz–1 MHz) is shown in Fig. 3. The value of the dielectric constant (ϵ') is found to be higher at the low frequencies. There are different factors that are responsible for the higher values of dielectric constant (ϵ') including grain boundary defects, Fe^{2+} ions, oxygen vacancies, and the interfacial dislocation pileup [13, 14]. On increasing the frequency, a decrease in the dielectric constant was observed and it became nearly constant at higher frequencies. When at a specific frequency of the alternating field, the dipoles are unable to follow the AC field and they lag behind [10]. Therefore, there is a decrease in the polarization with the increase in frequency. Finally, it becomes constant

and gives rise to the relaxation phenomenon. According to Maxwell and Wagner [11], the space charge polarization is because of the inhomogeneous structural behavior of dielectric material. According to the Maxwell-Wagner model, the well-conducting grains are separated by the insulating and thin grain boundaries [12]. The grain boundaries are effective in the region of low frequency; hence, at low frequency, a high value of the dielectric constant is obtained. On the other hand, at high frequencies, the dielectric constant exhibits low values due to mismatch in the hopping frequency and the applied frequency where the polarization occurs at the interface due to hopping of electrons on the equivalent lattice sites, i.e., $\text{Fe}^{3+} \leftrightarrow \text{Fe}^{2+}$ and $\text{Al}^{3+} \leftrightarrow \text{Al}^{2+}$, respectively.

Figure 4 shows the variation of dielectric constant vs ferrite content in the PANI matrix. The dielectric constant of the composites was observed to be decreasing with the increase in the content of ferrite filler at fixed frequency as shown in Table 2.

3.3.2 Dielectric Loss (ϵ'')

The variation of dielectric loss (ϵ'') vs frequency is shown in Fig. 4. The dielectric loss (ϵ'') is directly dependent on the tangent loss ($\tan \delta$). The dielectric loss (ϵ'') decreases with an increase in the frequency, and it indicates the amount of energy dissipated in dielectric with the applied electric field. Owing to the insulating grain boundaries, the resistivity is large at the lower frequencies; hence, there is a need of more energy for the exchange of electrons between Fe^{3+} and Fe^{2+} ions. Therefore, a high value was recorded for dielectric loss (ϵ''). The conducting grains offer less resistance;

Fig. 3 Variation of dielectric constant (ϵ') vs applied field frequency of F, FP1, FP2, FP3, and PANI (PP)

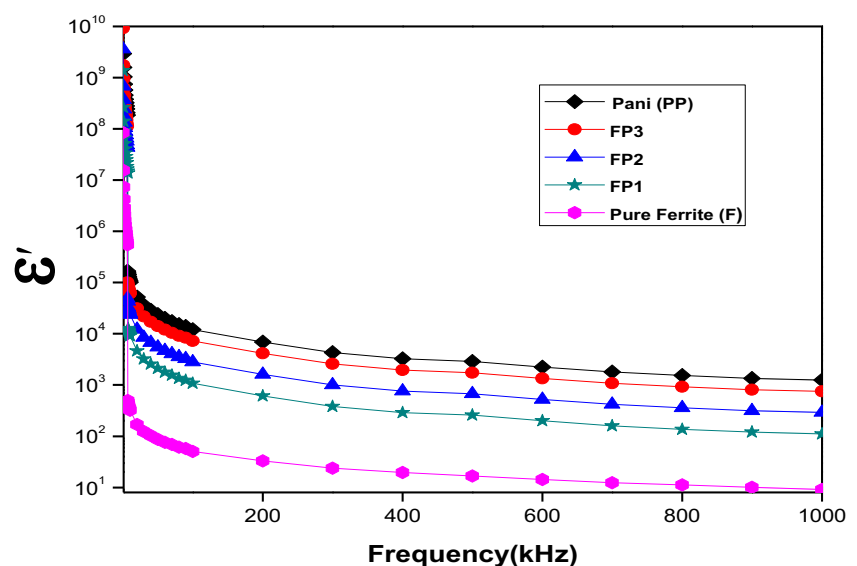
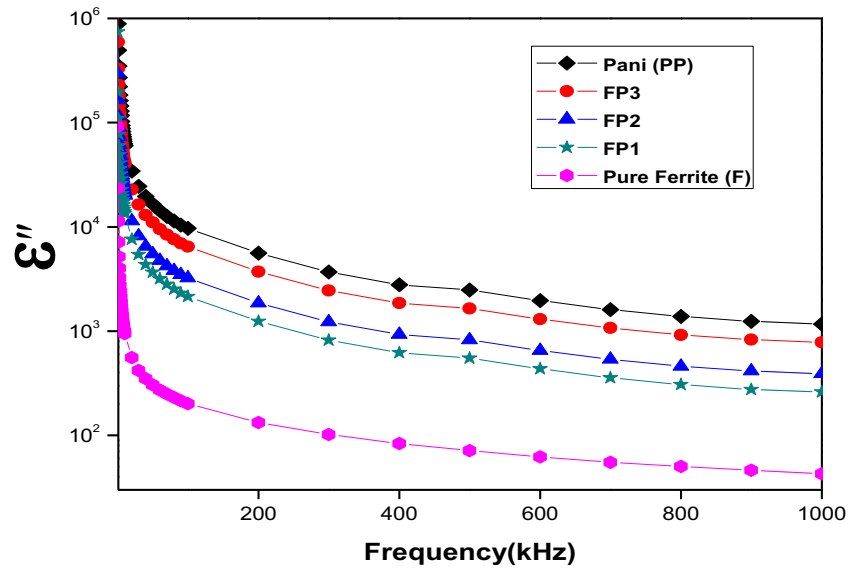


Fig. 4 Variation of dielectric loss factor (ϵ'') vs applied field frequency of F, FP1, FP2, FP3, and PANI (PP)



therefore, low values of dielectric loss (ϵ'') are observed in the high-frequency range.

3.3.3 Tangent Loss ($\tan \delta$)

The loss of tangent is determined by using the formula [13]

$$\tan \delta = \epsilon'' / \epsilon' \tag{5}$$

The variation of dielectric tangent loss ($\tan \delta$) vs high-frequency range (20 Hz to 1 MHz) is shown in Fig. 5. On the other hand, a high value of tangent loss is recorded in the low-frequency region. The tangent loss decreases with the increase in the field frequency, and it becomes almost independent at higher frequencies. The dielectric dispersion in ferrites is based on the Maxwell and Wagner model [14, 15] and Koop’s phenomenological theory [16]. Two phenomena initiate the dielectric loss in ferrites: (1) hopping of electrons and (2) charged defect dipoles. The dielectric loss is responsible for the hopping of electrons in the low-frequency range. In the high-frequency region, the dielectric loss is due to the reaction of defect dipoles to the applied field. With the increase in frequency, the relaxation of dipoles decreases

in the presence of an electric field. It eventually reduces the dielectric loss in the high-frequency region [17]. The impurities and imperfections in the structure of the crystal lattice may be responsible for this dielectric loss [18].

3.3.4 AC Electrical Conductivity (σ_{AC})

The following formula was used to calculate the AC conductivity of all the samples [15]:

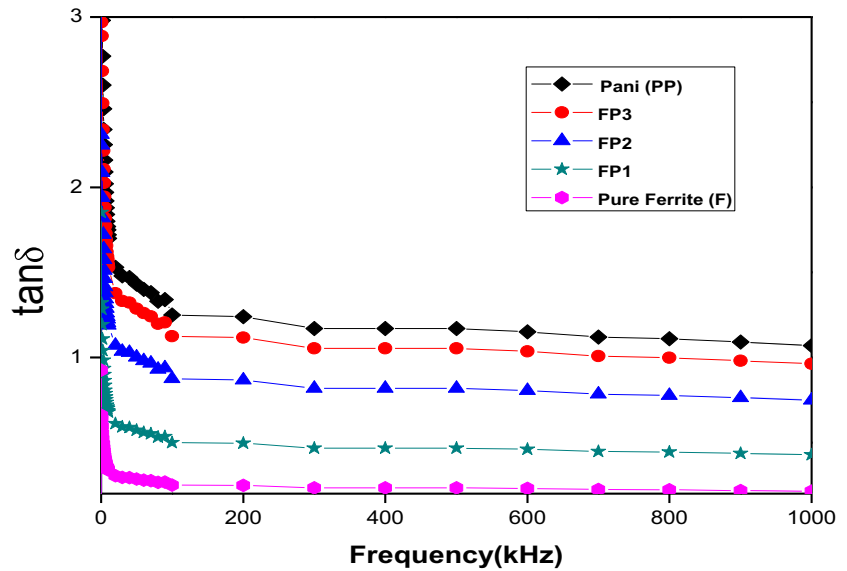
$$\sigma_{AC} = 2\pi f \epsilon_0 \epsilon'' \tag{6}$$

Figure 6 shows the variation in AC electrical conductivity (σ_{AC}) as a function of frequency. It is observed that in the higher-frequency range 20 Hz to 1 MHz the hopping of electrons between the ions of Fe^{3+} and Fe^{2+} at the octahedral sites is responsible for the AC conductivity (σ_{AC}) of the ferrite materials. With the increase in the frequency of the applied field, the frequency of electrons hopping between the Fe^{3+} and Fe^{2+} ions increased, thereby polarization increases and hence the AC conductivity (σ_{AC}) also increased. As explained by the Maxwell-Wagner model, there are conducting grains in the ferrite materials and

Table 2 The room temperature resistivity, activation energy, and dielectric properties of the synthesized samples

Samples	ρ (Ω cm) at room temp.	E_a (eV)	ϵ' at 1 MHz	ϵ'' at 1 MHz	$\tan \delta$	σ_{AC} (Ω cm) ⁻¹ at 1 MHz
PF	3.81×10^9	0.405	6.8851×10^1	4.2797×10^1	2.14×10^{-1}	-1.2948×10^{-1}
FP1	3.19×10^7	0.266	1.5495×10^3	2.6034×10^2	4.28×10^{-1}	-1.1143×10^{-1}
FP2	1.42×10^6	0.104	4.0677×10^3	3.9052×10^2	7.49×10^{-1}	-1.0737×10^{-1}
FP3	3.17×10^4	0.096	1.0459×10^4	7.8104×10^2	9.63×10^{-1}	-1.0044×10^{-1}
PANI	9.3×10^1	0.013	1.7432×10^4	1.1715×10^3	1.07×10^0	-9.6393×10^0

Fig. 5 Variation of dielectric tangent loss ($\tan \delta$) vs applied field frequency of F, FP1, FP2, FP3, and PANI (PP)



these grains are separated by thin layers of considerably resistive grain boundaries [19]. The grain boundary effect decreases the AC conductivity (σ_{AC}) at low frequency. However, the conducting behavior of grains is responsible for the dispersion behavior at high frequencies [20].

The power law explains the mutual relationship between the AC conductivity and frequency [21, 22].

$$\sigma_{tot}(\omega) = \sigma_{DC} + A\omega^n \tag{7}$$

where σ_{DC} stands for DC conductivity, n is the fractional exponent a dimensionless factor; and A is the pre-exponential factor with units of electrical conductivity. The electrical conductivity becomes equal to DC conductivity and independent of frequency as n reaches zero. When n is equal to or less than 1, the conductivity becomes dependent on frequency [23]. Therefore, the AC conductivity

can be considered as the sum of DC conductivity and AC conductivity across the insulator matrix.

3.4 Resistivity Measurement

3.4.1 Room Temperature Resistivity

The following relation was used to calculate the DC electrical resistivity [24]:

$$\rho = RA/d \tag{8}$$

where A stands for the area of the electrode in contact with the sample, d is the thickness of the sample, and R is the resistance of the sample. Table 2 shows the relationship between the resistivity of polyaniline at room temperature, Y-type ferrite $\text{CaBaCo}_2\text{Al}_{0.5}\text{Fe}_{11.5}\text{O}_{22}$, and ferrite-PANI

Fig. 6 Variation of AC electrical conductivity (σ_{AC}) vs applied frequency of F, FP1, FP2, FP3, and PANI (PP)

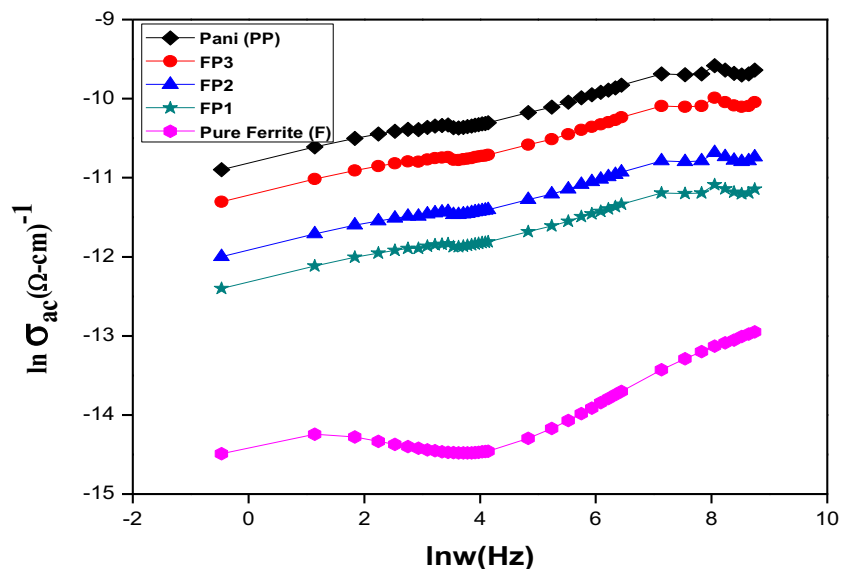
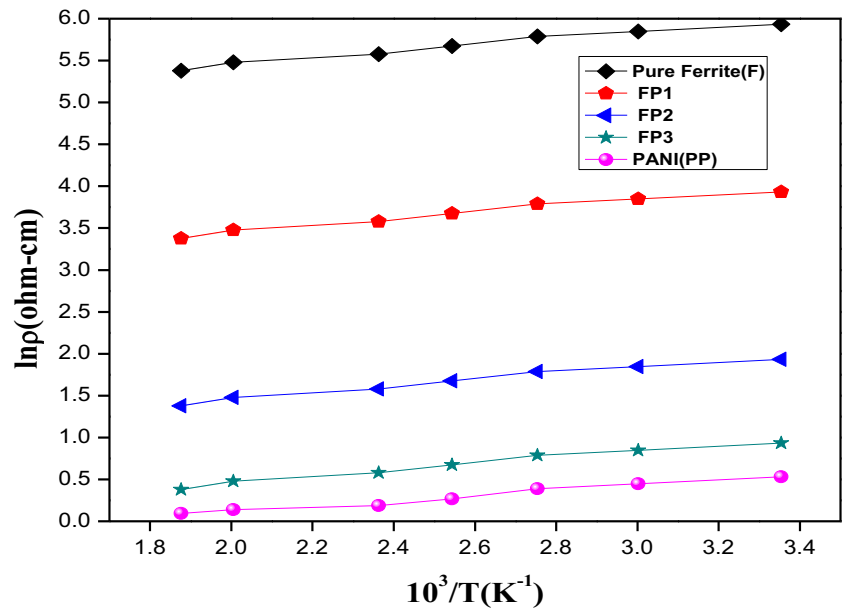


Fig. 7 Arrhenius plots for pure ferrite, FP1, FP2, FP3, and PANI (PP)



composites FP1, FP2, and FP3. The resistivity of PANI ($\rho = 9.3 \times 10^1 \Omega \text{ cm}$) is considerably low at room temperature. But, in the case of PANI as ferrite content in varying weight percentages of 75, 50, and 25%, there is an increase in the resistivity of composites from 3.17×10^4 to 3.19×10^7 ($\Omega \text{ cm}$). The resistivity of ferrite measures $3.81 \times 10^9 \Omega \text{ cm}$. Therefore, as compared with that of pure ferrite, the resistivity of ferrite-PANI composites increases with an increase in the content of ferrite. The particle blockage of the conduction path by ferrite nanoparticles, embedded in the PANI matrix, may be responsible for an increase in the resistivity of composites [21].

3.4.2 Temperature-Dependent Resistivity

Temperature-dependent resistivity of these samples was measured in the temperature range of 303–483 K. Figure 7 shows that the DC resistivity decreases linearly with temperature for all the samples. This can be attributed to the increase in drift mobility of thermally activated charge carriers [22]. The observed decrease in DC resistivity with temperature is normal behavior for ferrite which resembles with semiconducting behavior that follows the Arrhenius relation [21]:

$$\sigma_{\text{DC}} = \sigma_0 \exp(-E_a/kT) \tag{9}$$

where E_a stands for activation energy, σ_0 is a temperature-dependent term, and k is the Boltzmann constant. The conduction mechanism is due to both, i.e., mobility of electrons and holes. The mobility of holes increases with temperature

as it involves the thermal activation process and as result the resistivity starts to decrease. The decrease in resistivity with increased temperature for the synthesized materials is in agreement with already reported results [23, 24].

3.4.3 Activation Energy

Equation (9) was used to calculate the activation energies from the slopes of Arrhenius curves.

Taking into account the composition, the behavior of the electrical resistivity and the activation energy have been observed to be similar which is indicated in Table 2. The samples having higher values of activation energies have higher resistivity and vice versa [25]. From the higher values of activation energy for the high ferrite content, it can be inferred that the ferrite nanoparticles embedded in polyaniline matrix give rise to blockage in the conduction mechanism.

4 Conclusions

- The results of X-ray diffraction confirm the formation of a single-phase Y-type hexagonal structure.
- The dielectric constant (ϵ') of the ferrite-polymer decreases as the ferrite content increases; it is due to the high dielectric constant of ferrite as compared with that of polyaniline. The dielectric behavior follows the Maxwell-Wagner model, owing to interfacial polarization.
- For all the samples, the tangent loss and dielectric loss ($\tan \delta$) and complex dielectric loss (ϵ'') show normal behavior of dielectric with frequency.

- The increase in ferrite concentration leads to a drastic increase in the resistivity of the composites at room temperature.
- The activation energy and resistivity plots show similar behavior which shows that the samples with high resistivity have high activation energy and vice versa.
- Owing to the high value of the dielectric constant and enhanced resistivity of the composites, these samples may be suitable candidates for microwave absorption devices.

References

1. Stabik, J., Dybowska, A., Pluszyński, J., Szczepanik, M., Suchoń, Ł.: Magnetic induction of polymer composites filled with ferrite powders. *Arch. Mater. Sci. Eng.* **41**, 13–20 (2010)
2. Li, B.W., Shen, Y., Yue, Z.X., Nan, C.W.: Influence of particle size on electromagnetic behavior and microwave absorption properties of Z-type Ba-ferrite/polymer composites. *J. Magn. Magn. Mater.* **313**, 322–328 (2007)
3. Deng, J., He, C., Peng, Y., Wang, J., Long, X., Li, P., Chan, A.S.C.: Magnetic and conductive Fe₃O₄-polyaniline nanoparticles with core-shell structure. *Synth. Met.* **139**, 295–301 (2003)
4. Singh, K., Ohlan, A., Bakhshi, A.K., Dhawan, S.K.: Synthesis of conducting ferromagnetic nanocomposite with improved microwave absorption properties. *Mater. Chem. Phys.* **119**, 201–207 (2010)
5. Dhawan, S.K., Singh, K., Bakhshi, A.K., Ohlan, A.: Conducting polymer embedded with nanoferrite and titanium dioxide nanoparticles for microwave absorption. *Synth. Met.* **159**, 2259–2262 (2009)
6. Xu, F., Bai, Y., Jiang, K., Qiao, L.-J.: Characterization of a Y-type hexagonal ferrite-based frequency tunable microwave absorber. *Int. J. Miner. Metall. Mater.* **19**, 453–456 (2012)
7. Gairola, S.P., Verma, V., Kumar, L., Dar, M.A., Annapoorni, S., Kotnala, R.K.: Enhanced microwave absorption properties in polyaniline and nano-ferrite composite in X-band. *Synth. Met.* **160**, 2315–2318 (2010)
8. Abbas, S.M., Dixit, A.K., Chatterjee, R., Goel, T.C.: Complex permittivity, complex permeability and microwave absorption properties of ferrite-polymer composites. *J. Magn. Magn. Mater.* **309**, 20–24 (2007)
9. Apesteguy, J.C., Jacobo, S.E.: Synthesis of a soluble polyaniline-ferrite composite: magnetic and electric properties. *J. Mater. Sci.* **42**, 7062–7068 (2007)
10. Tanrıverdi, E.E., Uzumcu, A.T., Kavas, H., Demir, A., Baykal, A.: Conductivity study of polyaniline-cobalt ferrite (PANI-CoFe₂O₄) nanocomposite. *Nano-Micro Lett.* **3**, 99–107 (2011)
11. Aen, F., Niazi, S.B., Islam, M.U., Ahmad, M., Rana, M.U.: Effect of holmium on the magnetic and electrical properties of barium based W-type hexagonal ferrites. *Ceram. Int.* **37**, 1725–1729 (2011)
12. Abbas, S.M., Dixit, A.K., Chatterjee, R., Goel, T.C.: Complex permittivity, complex permeability and microwave absorption properties of ferrite-polymer composites. *J. Magn. Magn. Mater.* **309**, 20–24 (2007)
13. Gandhi, N., Singh, K., Ohlan, A., Singh, D.P., Dhawan, S.K.: Thermal, dielectric and microwave absorption properties of polyaniline-CoFe₂O₄ nanocomposites. *Compos. Sci. Technol.* **71**, 1754–176 (2011)
14. Devi, D.S.P., Bipinbal, P.K., Jabin, T., Kutty, S.K.N.: Enhanced electrical conductivity of polypyrrole/polypyrrole coated short nylon fiber/natural rubber composites prepared by in situ polymerization in latex. *Mater. Des.* **43**, 337–347 (2013)
15. Patil, R., Roy, A.S., Anilkumar, K.R., Jadhav, K.M., Ekhelkar, S.: Dielectric relaxation and ac conductivity of polyaniline-zinc ferrite composite. *Compos. Part B* **43**, 3406–3411 (2012)
16. Ashiq, M.N., Iqbal, M.J., Gul, I.H.: Structural, magnetic and dielectric properties of Zr-Cd substituted strontium hexaferrite (SrFe₁₂O₁₉) nanoparticles. *J. Alloys Compd.* **487**, 341–345 (2009)
17. Ajmal, M., Islam, M.U., Ashraf, G.A., Nazir, M.A., Ghouri, M.I.: The influence of Ga doping on structural magnetic and dielectric properties of NiCr_{0.2}Fe_{1.8}O₄ spinel ferrite. *Phys. B: Condens. Matter.* (2017). <https://doi.org/10.1016/i.phyb.2017.05.044>
18. Ishaque, M., Islam, M.U., Khan, M.A., Rahman, I.Z., Genson, A., Hampshire, S.: Structural, electrical and dielectric properties of yttrium substituted nickel ferrites. *Phys. B Condens. Matter* **405**, 1532–1540 (2010)
19. Gandhi, N., Singh, K., Ohlan, A., Singh, D.P., Dhawan, S.K.: Thermal, dielectric and microwave absorption properties of polyaniline-CoFe₂O₄ nanocomposites. *Compos. Sci. Technol.* **71**, 1754–1760 (2011)
20. Ajmal, M., Islam, M.U.: Structural, optical and dielectric properties of polyaniline-Ni_{0.5}Zn_{0.5}Fe₂O₄ nano-composites. *Phys. B Condens. Matter* **521**, 355–360 (2017)
21. Mangalaraja, R.V., Manohar, P., Gnanam, F.D., Awano, M.: Electrical and magnetic properties of Ni_{0.8}Zn_{0.2}Fe₂O₄/silica composite prepared by sol-gel method. *J. Mater. Sci.* **39**, 2037–2042 (2004)
22. Apesteguy, J.C., Jacobo, S.E.: Synthesis of a soluble polyaniline-ferrite composite: magnetic and electric properties. *J. Mater. Sci.* **42**, 7062–7068 (2007)
23. Reddy, P.V., Rao, T.S.: Dielectric behaviour of mixed Li-Ni ferrites at low frequencies. *J. Less-Common Met.* **86**, 255–261 (1982)
24. Batoo, K.M., Kumar, S., Lee, C.G.: Influence of Al doping on electrical properties of Ni-Cd nano ferrites. *Curr. Appl. Phys.* **9**, 826–832 (2009)
25. Hussain, S., Maqsood, A.: Structural and electrical properties of Pb-doped Sr-hexa ferrites. *J. Alloys Compd.* **466**, 293–298 (2008)